Iranian Journal of Materials Forming 12 (3) (2025) 42-55

Online ISSN: 2383-0042

IJMF

Iranian Journal of Materials Forming

Journal Homepage: http://ijmf.shirazu.ac.ir

Research Article

Micromechanical Modeling of Two-Way Shape Memory Response of Semi-Crystalline Polymers Based on Equivalent Inclusion Method

M. Bakhtiari and K. Narooei*

Department of Materials Science and Engineering, K. N. Toosi University and Technology, Tehran, Iran

ARTICLE INFO

Article history:

Received 16 June 2025
Reviewed 26 July 2025
Revised 31 July 2025
Accepted 9 August 2025

Keywords:

Shape memory polymers
Micromechanics modeling
Quasi two-way SME
Equivalent inclusion method
Mori-Tanaka model

Please cite this article as:

Bakhtiari, M., & Narooei, K. (2025). Micromechanical modeling of two-way shape memory response of semi-crystalline polymers based on equivalent inclusion method. *Iranian Journal of Materials Forming*, *12*(3), 42-55. https://doi.org/10.22099/IJMF.2025.53516.1335

ABSTRACT

Two-way shape memory polymers (2W-SMPs) are a class of intelligent materials that demonstrate reversible form memory, rendering them suitable for a wide range of applications in response to external stimuli. During the phase transition in the shape memory cycle of semi-crystalline polymers, the 2W-SMPs are represented as a two-phase material, consisting of an amorphous matrix and the crystalline inclusions. This paper employs the Equivalent Inclusion Method (EIM), based on the Modified-Mori-Tanaka (MMT) approach, to determine the effective thermomechanical response of inclusions inside a heterogeneous matrix. Unlike existing phase transition models, the proposed model accounts for both phase interactions and the morphology (shape and size) of the inclusion phase throughout the thermomechanical cycle. The model was implemented using the UMAT user subroutine in ABAQUS to simulate the mechanical behavior of SMPs. Analysis of various inclusion shapes revealed that ellipsoidal shapes most accurately represent the morphology of the inclusion phase. In particular, a highly elongated ellipsoidal inclusion (a/c = 1/25) provided the best agreement with simulation results. A fivefold increase in the (a/c) aspect ratio of the crystalline inclusions resulted in approximately 10% increase in crystallization-induced strain, thereby improving consistency with shape memory experiments when the actual morphology was considered. The shape memory response of PCL under a stress of 250 kPa demonstrated a ~12.5% strain increase during cooling from 65 to -40℃, with about 7% occurring near the crystallization point over a 40℃ interval. Incorporating phase interactions significantly enhanced the model's agreement with experimental results on shape recovery.

1. Introduction

A stimuli-responsive materials called shape memory polymers (SMPs) can be trained into a temporary shape and subsequently return to their pre-programmed shape in response to external stimuli like heat, light, or electricity [1-3]. Compared to shape memory alloys (SMAs) and ceramics, SMPs offer several advantages, including lower density, adjustable mechanical properties, and the ability for large reversible deformations [4, 5]. These properties have attracted great interest in their applications in various fields, such as deployable aerospace structures, biomedical implants, and self-healing systems [6, 7]. Beyond the traditional

* Corresponding author
E-mail address: knarooei@kntu.ac.ir (K. Narooei)
https://doi.org/10.22099/IJMF.2025.53516.1335

one-way shape memory polymers (1W-SMPs), which return to their original shape only once after activation, researchers have also developed two-way shape memory polymers (2W-SMPs) that can reversibly switch between two different shapes without the need for external reprogramming [8].

A variant known as quasi two-way shape memory effect (quasi 2W-SME) describes SMPs that show reversible deformation during the cooling and heating cycle under a constant external mechanical load. This characteristic makes quasi-two-way SMPs particularly valuable for practical applications, providing an efficient and adaptable way for reversible motion control [9, 10]. As a result, they are increasingly used in soft robotic systems, adjustable grasping devices, and responsive medical implants that require reliable and repetitive shape-changing ability [11].

During the last two decades, two main categories of thermomechanical constitutive models have been developed to describe shape memory behavior: rheological and phenomenological models [12-14]. Early modeling efforts used simple viscoelastic components, such as springs and dashpots, to represent the material's behavior based on the viscous and elastic properties of SMPs [15, 16]. Later, a phenomenological approach based on phase transition was developed to capture the thermomechanical behavior of epoxy-based shape memory polymers [17]. This model assumed that the material consists of two distinct phases: a frozen phase and an active phase. The main mechanism is the storage of strain energy in the frozen phase, which governs both the recovery processes and shape fixation. While this framework effectively described material behavior under small deformation, it was subsequently modified by adding an additional structural phase (hard phase) to better represent the response of shape memory polyurethanes under larger strains. These improvements extended the model's ability to predict complex shape memory behavior in different material systems and loading conditions [18].

Micromechanical theory provides an alternative perspective for modeling the shape memory behavior of SMPs by directly considering their microstructure [19]. It serves as a crucial link between the macroscopic behavior of multi-phase systems and the intrinsic properties of their individual material components [9]. Establishing this relationship enables accurate predictions of the performance of multiphase materials, making micromechanics a central topic of research for decades. Through appropriate micromechanical homogenization techniques, effective material properties can be derived from the characteristics of each phase, which is vital for optimizing the design of multiphase systems. From a micromechanical standpoint, inclusions are typically modeled as being embedded within an infinite, homogeneous, isotropic elastic matrix, changing in shape and size during transformations [20].

The two most basic homogenization models are the Voigt model [21] and the Reuss model [22]. Collectively known as the rule of mixtures (RoM), the Voigt model assumes a uniform strain field within the representative volume element (RVE), implying that both the matrix and inclusions undergo the same strain. In contrast, the Reuss model assumes a uniform stress field within the RVE, such that all phases experience the same stress level. However, both models neglect the effect of inclusion shape or orientation, and do not account for interactions between inclusions within the matrix. Consequently, these methods are unsuitable for systems with a high volume fraction of inclusion. Nonetheless, they provide theoretical upper and lower bounds for effective properties, which no other model can surpass. Beyond the Voigt and Reuss approaches, most mean-field homogenization methods are based on Eshelby's basic work, with the Mori-Tanaka model being one of the most widely adopted [23, 24].

Within micromechanics theory, to homogenize a heterogeneous material and eliminate the source of heterogeneity, the heterogeneous region is conceptually replaced with an equivalent inclusion in which an appropriately distributed eigenstrain is introduced [25]. By this replacement, the material's elastic properties are effectively homogenized. In this way the macroscopic behavior of heterogeneous materials can be directly related to their microstructural composition through

micromechanical modeling [26]. This framework relies on the concept of an RVE, which captures the material's microstructure by accounting for the geometry and mechanical properties of its constituent phases [27, 28]. Micromechanics methods are generally divided into two broad categories: homogenization methods and average field theories. The average field approach estimates the macroscopic mechanical response of heterogeneous materials by considering averaged stress and strain fields at the microscale. This approach, originally proposed by Eshelby, later gave rise to more advanced schemes such as the self-consistent method and the Mori-Tanaka methods [29, 30]. The shape memory behavior of thermally activated SMPs is influenced by complex interactions, including the polymer's structure morphology, programming conditions, and recovery parameters [31]. A phase evolution methodology was originally formulated for SMAs to model their pseudo-elastic thermomechanical response and stress-induced phase transformations [24]. This framework has since been adapted to SMPs to capture their thermomechanical behavior. In semi-crystalline SMPs, the material properties are determined by the degree of crystallinity as well as the the size and orientation of the crystalline and amorphous phases [32].

To the authors' knowledge, only a limited number of studies have addressed the modeling of both the one-way and two-way shape memory effects in semi-crystalline polymers [33-35]. While these models successfully predict the temperature-stress-strain responses of crosslinked poly(ε-caprolactone) (PCL) during both shape memory cycles, they do not account for microstructural characteristics such as the shape and size of crystalline phases, which evolve and reorient during cooling and heating. To more accurately describe the deformation behavior of shape memory polyurethane (SMPU) materials, Kim et al. [36] proposed a three-phase phenomenological model consisting of a hard segment phase and two soft segment phases (active and frozen). Subsequently, Gilormini and Diani [37] addressed an unresolved issue from the earlier work of Chen and Lagoudas's [38] by integrating Liu et al.'s model with homogenization techniques, thereby overcoming the limitations of the uniform stress assumption. These advances in multiphase material theory have allowed researchers to estimate the effective elastic properties of SMPs by treating them as two-phase systems. More recently, micromechanical modeling has been applied to 1W-SMPs, where the effect of microstructural features has been investigated using the Modified Mori-Tanaka method (MMT) [19]. However, to date, no study has examined micromechanical modeling of quasi-two-way shape memory effects in semi-crystalline SMPs over a complete thermomechanical cycle.

The primary objective of this study is to establish a micromechanical constitutive model for two-way shape memory polymers under applied stress conditions. In particular, the work examines the relationship between macroscopic variables, such as applied stress and shape memory response and microscopic features, including the size and morphology of microstructural constituents, by utilizing the equivalent inclusion method (EIM) in combination with the Modified-Mori-Tanaka (MMT) approach. The proposed framework further accounts for the interactions among different phases throughout the cooling/heating cycle. Model predictions were systematically validated against available experimental data, confirming the reliability of the approach.

2. Constitutive Micromechanics Model

Crosslinked semi-crystalline networks exhibited the ability to undergo a spontaneous and reversible transition between two different configurations when subjected to thermal cycling [10]. Achieving two-way shape memory effects (2W-SMEs) requires the coexistence of both crystalline and amorphous phases. The connection between the macro and micro-scale configuration of semi-crystalline SMP is illustrated in Fig. 1. At the meso-scale, Fig. 1(b) presents a three dimensional representative volume element (3D-RVE), showing the simultaneous presence of crystalline and amorphous phases. At the micro-scale, semi-crystalline SMPs consist of an amorphous matrix and embedded crystalline phases, as illustrated in Fig. 1(c, d). When subjected to mechanical loading, crystalline domains tend to align

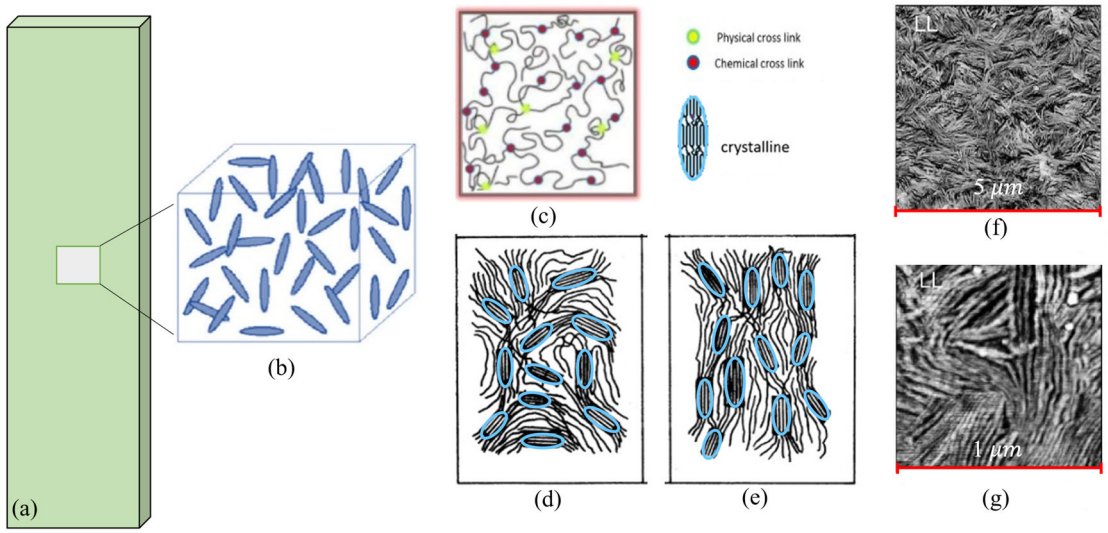

Fig. 1. (a) Schematics representation of a semi-crystalline polymer at the macro-scale, (b) 3D-RVE at the meso-scale, micro-scale configuration of (c) amorphous phase, (d) random state crystalline phase, (e) oriented crystalline phase, and (f, g) atomic force microscopy (AFM) images including the coexistence of crystalline and amorphous phases [40].

along the direction of the applied stress [39]. Furthermore, as depicted in Fig. 1 (f, g), experimental observations reveal that polymers often contain distinct domains corresponding to different phases [40, 41]. The mechanical response of semi-crystalline polymers, particularly that of the crystalline phase, is typically modeled as fully elastic. This behavior is strongly influenced by several factors, including temperature, crystalline volume fraction, degree of crosslinking, and microstructural characteristics such as entanglement, crystalline size, shape, and spatial distribution [32, 40].

Fig. 2 displays a schematic representation of a typical two-way thermomechanical cycle for a two-phase SMP. The 2W-SME can be described as follows: (1) the sample is first heated to acquire shape "A" at elevated temperatures, (2) subsequently deformed under external load to shape "B", (3) upon cooling close to the crystallization temperature it transforms into shape "C", (4) further cooling results in shape "D", and (5) reheating above the melting temperature drives recovery back to shape "B". During cooling step, the transformation from "B" to "D" occurs through crystallization-induced elongation under constant external stress, whereas the reverse transformation from "D" to "B" during heating is governed by melting-induced contraction. Fig. 3(a) illustrates the deformation of the RVE adopted in this model throughout the 2W shape memory cycle. For micromechanical modeling, the 3D-RVE is considered to comprise an amorphous matrix and crystalline inclusion phases. Correspondingly, Fig. 3(b) schematically depicts the evolution of crystallinity during the 2W-SME process, based on prior studies and differential scanning calorimetry (DSC) results for semi-crystalline polymers [32]. Due to the absence of detailed microstructural data, certain modeling assumptions were made in the modeling approach [41]. The macroscopic response was through homogenization, providing the effective stresses and strains acting on the equivalent homogeneous material sample [42]. The proposed constitutive framework thus incorporates phase transition mechanisms, namely crystallization and melting, under constant loading during heating and cooling cycles while accounting for the microstructural characteristics of semi-crystalline 2W-SMPs.

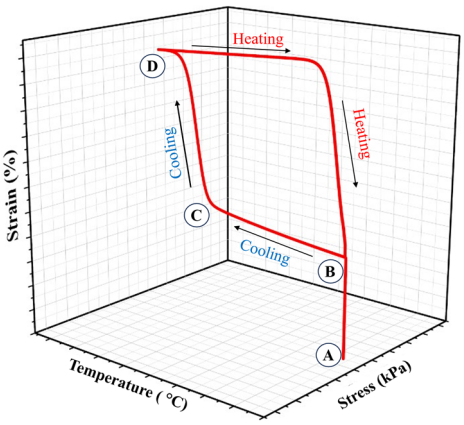

Fig. 2. Schematic representation of a typical two-way thermomechanical cycle in a two-phase SMP.

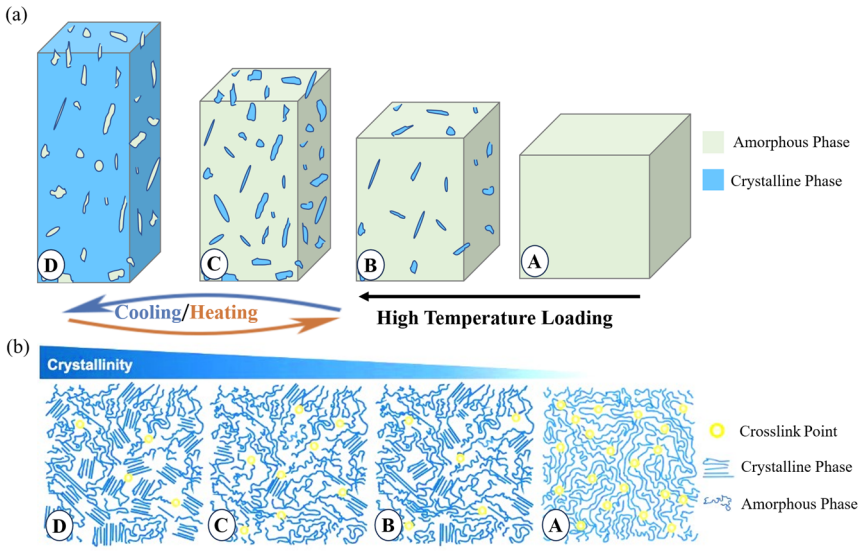

Fig. 3. (a) Schematic representation of the RVE corresponding to shapes (A)-(D) in Fig. 2, and (b) crystallinity content in a 2W-SMP during reversible cooling and heating.

2.1. Description of micromechanics-based model

In the present two-phase micromechanical framework, the crystalline phase is treated as the inclusion phase embedded within the amorphous matrix. Figs. 4(a) and (b) show the 2D and 3D RVEs of two-phase semi-crystalline 2W-SMP, respectively. Microstructure observations, presented in Fig. 4, indicate that the crystalline regions (highlighted in yellow) can be approximated as ellipsoidal shapes [43]. Consequently, in the model, the inclusions are represented as ellipsoidal shapes embedded within the amorphous matrix [41, 43, 44]. Furthermore, Fig. 5(c) presents a 2D schematic of an ellipsoid-inclusion within a homogeneous SMP matrix. In Fig. 5(c), $\mathbb{C}^I$ and $\mathbb{C}^M$ denote the fourth-order elastic stiffness tensors of the inclusion and the matrix, respectively. Considering the SMP as a two-phase material (see Fig. 5(c)) subjected to a uniform far-field stress ($\bar{\boldsymbol{\sigma}}$), applied at infinity, the stress-strain relation for a homogeneous comparison material with amorphous elasticity can be expressed as:

$$\bar{\boldsymbol{\sigma}} = \mathbb{C}^M : (\boldsymbol{\varepsilon}^0) \tag{1}$$

Here $\boldsymbol{\varepsilon}^0$ represents the corresponding uniform strain. Due to differences in mechanical properties (e.g., stiffness), geometry, and loading conditions, stress and strain are redistributed between the matrix and the inclusions. This redistribution induces interactions between the two phases, which are captured; through the introduction of the interaction strain ($\tilde{\boldsymbol{\varepsilon}}$) [20]. The mismatch in deformation between the matrix and the inclusions generates additional internal stress and strain fields. These fields arise not only from externally applied load but also from the mechanical interactions between the constituent phases, commonly referred to as interaction strain [19]. Consequently, when the two-phase system is subjected to a far-field stress, $\bar{\boldsymbol{\sigma}}$, the presence of the inclusions modifies the mean stress in the matrix by inducing a mean interaction stress $\tilde{\boldsymbol{\sigma}}$, corresponding to a mean interaction strain, $\tilde{\boldsymbol{\varepsilon}}$. This relation can be expressed as:

$$\boldsymbol{\sigma}^M = \bar{\boldsymbol{\sigma}} + \tilde{\boldsymbol{\sigma}} = \mathbb{C}^M : (\boldsymbol{\varepsilon}^0 + \tilde{\boldsymbol{\varepsilon}}) \tag{2}$$

Where the interaction stress and strain are related by:

$$\tilde{\boldsymbol{\sigma}} = \mathbb{C}^M : \tilde{\boldsymbol{\varepsilon}} \tag{3}$$

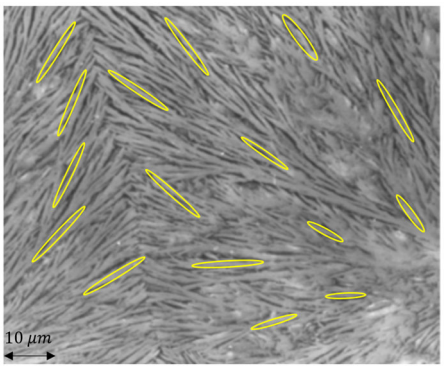

Fig. 4. Atomic force microscopy (AFM) image illustrating the microstructure of polypropylene as a representative semi-crystalline polymer [43].

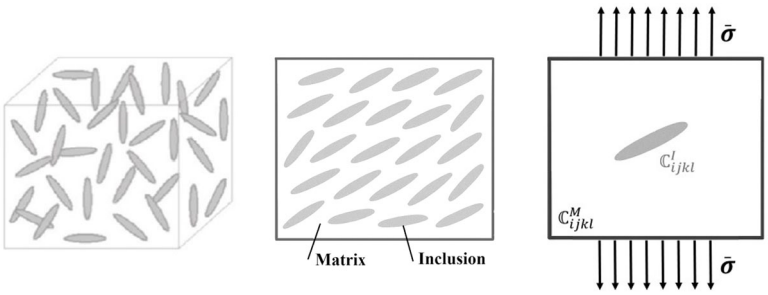

Fig. 5. (a) 3D, and (b) 2D RVE in the micromechanics model of a semi-crystalline 2W-SMP, and (c) schematic of an ellipsoid-inclusion embedded in the homogenous SMP matrix under applied stress.

By assuming a uniform inclusion stress ($\boldsymbol{\sigma}^I$) and strain within the inclusion, in addition to the matrix phase response, a perturbation strain (and corresponding stress) field must be introduced to account for the presence of inhomogeneities within the composite [45]:

$$\boldsymbol{\sigma}^I = \bar{\boldsymbol{\sigma}} + \tilde{\boldsymbol{\sigma}} + \boldsymbol{\sigma}^{pt} = \mathbb{C}^M : (\boldsymbol{\varepsilon}^0 + \tilde{\boldsymbol{\varepsilon}} + \boldsymbol{\varepsilon}^{pt}) \tag{4}$$

Where $\boldsymbol{\sigma}^{pt}$ and $\boldsymbol{\varepsilon}^{pt}$ represent the uniform perturbation stress and strain fields within the inclusions, respectively. For a finite volume fraction of inclusions, both the interaction strain between neighboring inclusions ($\tilde{\boldsymbol{\varepsilon}}$) and the perturbation strain ($\boldsymbol{\varepsilon}^{pt}$) caused by the inhomogeneity of the inclusions in the matrix must be considered [20, 45]. Accordingly, the average strain in the amorphous (matrix) and crystalline (inclusion) phases can be expressed as:

$$\bar{\boldsymbol{\varepsilon}}^M = \boldsymbol{\varepsilon}^0 + \tilde{\boldsymbol{\varepsilon}} - \boldsymbol{\varepsilon}^T \tag{5}$$

$$\bar{\boldsymbol{\varepsilon}}^I = \boldsymbol{\varepsilon}^0 + \tilde{\boldsymbol{\varepsilon}} + \boldsymbol{\varepsilon}^{pt} - \boldsymbol{\varepsilon}^T - \boldsymbol{\varepsilon}^{in} \tag{6}$$

Here $\bar{\boldsymbol{\varepsilon}}^M$ and $\bar{\boldsymbol{\varepsilon}}^I$ represent the average elastic strain in the matrix and inclusion phases, respectively, while $\boldsymbol{\varepsilon}^T$ represents the thermal strain, and $\boldsymbol{\varepsilon}^{in}$ corresponds to the inelastic storage/release strain in the cooling/heating of the inclusion phase. The inelastic strain generating during phase transition under actuation stress (external load), as observed in PCL-based SMPs, can be evaluated using the following expression [34]:

$$\dot{\boldsymbol{\varepsilon}}^{in} = \begin{cases} (\dfrac{\beta \dot{\xi}_c}{E_M T})\boldsymbol{\sigma}; & cooling:\ \dot{T} < 0 \\ \dfrac{\dot{\xi}_c}{\xi_c}\boldsymbol{\varepsilon}^{in}; & heating:\ \dot{T} > 0 \\ 0; & steady:\ \dot{T} = 0 \end{cases} \tag{7}$$

Here T and $\dot{T}$ are temperature and temperature rate, respectively. The parameter β represents the dependency of inelastic strain on the actuation stress, while $E_M T$ represents the temperature-dependent modulus of the amorphous (matrix) network. Furthermore, ξ_c denotes the volume fraction of the crystalline inclusion phase. Superscripts n and $n+1$ are used to indicate quantities evaluated at the previous time t_n and the current time step t_{n+1}, respectively. Accordingly, inelastic strain in time-discrete form can be expressed as:

$$\boldsymbol{\varepsilon}^{in}_{n+1} = \begin{cases} \boldsymbol{\varepsilon}^{in}_n + \beta(\xi^c_{n+1} - \xi^c_n)(\dfrac{\boldsymbol{\sigma}}{E_M T}); & cooling \\ \dfrac{1}{1 - \frac{\xi^c_{n+1} - \xi^c_n}{\xi^c_{n+1}}}\boldsymbol{\varepsilon}^{in}_n; & heating \\ 0; & steady \end{cases} \tag{8}$$

It is worth mentioning that the total thermal strain $\boldsymbol{\varepsilon}^T$ can be expressed in terms of the thermal expansion coefficients of each phase using the rule of mixture [46]:

$$\boldsymbol{\varepsilon}^T = \xi^I \boldsymbol{\varepsilon}^T_I + (1 - \xi^I)\boldsymbol{\varepsilon}^T_M = \left(\int_{T_0}^{T} (\xi^I \alpha^T_I + (1 - \xi^I)\alpha^T_M)\, dT\right)\boldsymbol{I} \tag{9}$$

Here $\boldsymbol{\varepsilon}^T_I$ and $\boldsymbol{\varepsilon}^T_M$ represent the thermal strains of the inclusion and matrix phases, respectively, while, α^T_I and α^T_M denote their corresponding thermal expansion coefficients. In Eq. (9), $\boldsymbol{I}$ is the second-order identity tensor, T_0 and T are the reference and current temperature, and ξ^I represents the crystalline volume fraction , which can be determined from the crystalline weight content as follows [11]:

$$\zeta_c = \begin{cases} \dfrac{\zeta^w_c}{1 + exp[\beta_c\, arctan(T^{eff}_c)(T - T^{eff}_c)]}; & cooling \\ \dfrac{\zeta^w_c}{1 + exp[\beta_m\, arctan(T^{eff}_m)(T - T^{eff}_m)]}; & heating \end{cases} \tag{10}$$

Where ζ_c^w is the maximum crystalline weight content, while β_c and β_m are positive material constants. T_c^{eff} and T_m^{eff} denote the effective crystallization and melting temperatures, respectively. To capture the evolution of the crystalline phase during thermal cycling, a physically based evolution law was proposed [11, 34]:

$$\xi_c = \frac{\rho_a \zeta_c}{\rho_a \zeta_c + \rho_c(1-\zeta_c)} \tag{11}$$

Where ρ_a and ρ_c denote the densities of the amorphous and crystalline phases, respectively. Experimental studies have demonstrated that crystallization is influenced by the applied stress tensor ($\boldsymbol{S}_{Eng}$), cooling (ν_c) and heating (ν_h) rates. Consequently, the effective transition temperatures for crystallization and melting can be expressed as [11]:

$$T_c^{eff} = T_c + \gamma_c^1 \left\|\boldsymbol{S}_{Eng}\right\| + \gamma_c^2 \frac{\nu_c}{\nu_c^R} \tag{12}$$

$$T_m^{eff} = T_m + \gamma_m^1 \left\|\boldsymbol{S}_{Eng}\right\| + \gamma_m^2 \frac{\nu_m}{\nu_m^R} \tag{13}$$

In Eqs. (12) and (13), γ_c^1, γ_m^1 and γ_c^2, γ_m^2 describe the effects of the actuation stress and thermal rate, respectively. ν_c^R, ν_m^R represent the reference cooling and heating rates, while $\left\|\boldsymbol{S}_{Eng}\right\|$ is the norm of the applied stress tensor ($\boldsymbol{S}_{Eng}$). Based on Hooke's law, the constitutive equation of the inclusion and matrix phases could be expressed by combining Eqs. (5) and (6) with the corresponding elastic stiffness tensor of each phase:

$$\bar{\boldsymbol{\sigma}}^M = \mathbb{C}^M : (\boldsymbol{\varepsilon}^0 + \tilde{\boldsymbol{\varepsilon}} - \boldsymbol{\varepsilon}^T) \tag{14}$$

$$\bar{\boldsymbol{\sigma}}^I = \mathbb{C}^I : \left(\boldsymbol{\varepsilon}^0 + \tilde{\boldsymbol{\varepsilon}} + \boldsymbol{\varepsilon}^{pt} - \boldsymbol{\varepsilon}^T - \boldsymbol{\varepsilon}^{in}\right) \tag{15}$$

Here $\bar{\boldsymbol{\sigma}}^M$ and $\bar{\boldsymbol{\sigma}}^I$ are the average stress tensors of the matrix and inclusion phase, respectively. Within the framework of the equivalent inclusion method (EIM), eigenstrain refers to a fictitious internal strain field introduced within an inclusion assumed to have the same elastic properties as the surrounding matrix. This approach serves to simulate the effect of a real inhomogeneous inclusion with different material properties. In doing so, the complex inhomogeneity problem is reduced to a mathematically tractable one involving a homogeneous medium with internal strain incompatibilities, thereby enabling the stress and strain fields to be analyzed through Eshelby's solution. Eshelby demonstrated that an inhomogeneity can be equivalently considered as an inclusion with the same elastic properties as the matrix, subjected to a corresponding perturbation strain, commonly referred to as eigenstrain. In the context of SMPs, eigenstrain represents the transition strain associated with the phase transitions in semi-crystalline SMPs during the shape memory cycle. Within this framework, the EIM provides a means to evaluate the perturbation strain by incorporating the eigenstrain ($\boldsymbol{\varepsilon}^*$). A fundamental requirement of the EIM is the consistency condition, which ensures equivalence between the real inhomogeneous inclusion and the fictitious homogeneous inclusion subjected to the prescribed eigenstrain. This condition enforces that the average stress within both inclusions remains identical under the same applied remote loading, thereby guaranteeing that the mechanical response of the simplified model accurately reflects that of the original two-phase composite structure [20].

$$\begin{aligned}\mathbb{C}^I : (\boldsymbol{\varepsilon}^0 + \tilde{\boldsymbol{\varepsilon}} + \boldsymbol{\varepsilon}^{pt} - \boldsymbol{\varepsilon}^T - \boldsymbol{\varepsilon}^{in}) \\ = \mathbb{C}^M : (\boldsymbol{\varepsilon}^0 + \tilde{\boldsymbol{\varepsilon}} + \boldsymbol{\varepsilon}^{pt} - \boldsymbol{\varepsilon}^T - \boldsymbol{\varepsilon}^{in} - \boldsymbol{\varepsilon}^*)\end{aligned} \tag{16}$$

The disturbance strain field in the matrix surrounding an inclusion can be expressed as the action of the Eshelby tensor on the total eigenstrain. This total eigenstrain accounts for all inelastic strain sources intrinsic to the inclusion, including thermal mismatch and phase transition effects [19, 24]. Accordingly, the disturbance strain ($\boldsymbol{\varepsilon}^{pt}$) of the inclusion is related to the total eigenstrain through the Eshelby tensor ($\boldsymbol{S}^I$) as [45]:

$$\boldsymbol{\varepsilon}^{pt} = \boldsymbol{S}^I : \left(\boldsymbol{\varepsilon}^* + \boldsymbol{\varepsilon}^T + \boldsymbol{\varepsilon}^{in}\right) \tag{17}$$

The Eshelby tensor depends on the inclusion aspect ratio (i.e., the size and shape effect of the inclusion) as well as the Poisson's ratio of the surrounding matrix [19]. By evaluating the average stress within both the matrix and the inclusion, the overall effective stress in the two-phase material system can then be obtained as follows [20]:

$$\bar{\boldsymbol{\sigma}} = \xi^I \bar{\boldsymbol{\sigma}}^I + (1-\xi^I)\bar{\boldsymbol{\sigma}}^M \tag{18}$$

By substituting Eqs. (14) and (15) in (18), the volume average stress can be expressed as:

$$\mathbb{C}^M : \tilde{\boldsymbol{\varepsilon}} + \xi^I \mathbb{C}^I : \boldsymbol{S}^I : \left(\boldsymbol{\varepsilon}^* + \boldsymbol{\varepsilon}^T + \boldsymbol{\varepsilon}^{in}\right) = 0 \tag{19}$$

The average strain and average stress are related to the equivalent stiffness tensor as follows [19]:

$$\bar{\boldsymbol{\sigma}} = \bar{\mathbb{C}} : \bar{\boldsymbol{\varepsilon}} \tag{20}$$

In the homogenization step, the inclusion is regarded as a part of the matrix while carrying the eigenstrain. By employing effective elastic stiffness tensors, this approach establishes a relationship between the volume averages of stress and strain within the SMP. The Mori–Tanaka method introduces the strain concentration tensor by assuming that each inclusion experiences the matrix average strain rather than the macroscopic average strain of the composite [23]. This assumption more reflects the physical environment surrounding inclusions, particularly in matrix-dominated composites, while preserving analytical tractability. Accordingly, Mori-Tanaka proposed that, for a two-phase microstructure with multiple identical inclusions, the relationship between the average strains of the inclusion and the matrix can be expressed as [23]:

$$\bar{\boldsymbol{\varepsilon}}^I = \boldsymbol{A}^{MT} : \bar{\boldsymbol{\varepsilon}}^M \tag{21}$$

Where $\boldsymbol{A}^{MT}$ or the Mori–Tanaka strain concentration tensor is a fourth-order tensor that provides a mean-field approximation linking the average inclusion strain to the surrounding matrix strain. The primary objective is to construct a concentration tensor that can relate the average stress or strain within the inclusion to the imposed boundary conditions. The fundamental formulation of the Mori–Tanaka method, as derived in our previous work [19], is given by:

$$\boldsymbol{A}^{MT} = \left[\boldsymbol{I}^{(4)} + \boldsymbol{S}^I : (\mathbb{C}^M)^{-1} : (\mathbb{C}^I - \mathbb{C}^M)\right]^{-1} \tag{22}$$

Here, $\boldsymbol{I}^{(4)}$ is the fourth-order identity tensor. Based on the Mori-Tanaka method and Eshelby solution for two-phase systems, the effective stiffness tensor can be obtained from the volume fraction of inclusion and the elastic stiffness tensors of matrix and inclusion as [19]:

$$\bar{\mathbb{C}} = [(1-\xi^I)\mathbb{C}^M + \xi^I \mathbb{C}^I \boldsymbol{A}^{MT}] : [\xi^I \boldsymbol{A}^{MT} + (1-\xi^I)\boldsymbol{I}^{(4)}]^{-1} \tag{23}$$

The overall average stress tensor, accounting for applied, thermal, and inelastic strains, is then expressed as:

$$\bar{\boldsymbol{\sigma}} = \bar{\mathbb{C}} : \left(\boldsymbol{\varepsilon}^0 - \boldsymbol{\varepsilon}^{in} - \boldsymbol{\varepsilon}^T\right) \tag{24}$$

It is essential to note that the present constitutive model was implemented in the UMAT user subroutine of the ABAQUS software. Employing the MMT method, the proposed micromechanical model successfully predicts the effective macroscopic behavior of quasi-2W-SMPs throughout the shape memory cycle.

3. Results and Discussion

To evaluate the validity of the proposed framework developed in the previous section, a series of simulations was conducted and compared with results available in the literature [34, 47]. These studies encompass a wide range of shape recovery processes and structural configurations, thereby providing the validity basis for assessing the robustness of the presented model. For this purpose, the model was implemented using the user-defined subroutine UMAT in ABAQUS. It was applied to simulate a uniaxial shape memory cycle comprising three sequential steps: loading under fixed external load at a high temperature (T_h), cooling under constant stress down to a low temperature (T_l), and reheating under constant external force conditions to enable shape recovery. The material parameters adopted in these simulations are summarized in Table 1.

To verify the proposed model, the numerical simulations were performed under uniaxial loading conditions. Fig. 6 illustrates the geometry of the SMP sample and the corresponding boundary conditions imposed throughout the 2W shape memory cycle. A force control approach was adopted, where a uniaxial tensile force was applied to the sample. Symmetry conditions were enforced by constraining the displacements in the normal directions of the back, bottom, and right faces of the modeled geometry. In the

first step, loading at high temperature, a traction force was applied to ensure fixed-stress boundary conditions, as shown in Fig. 7. During the second step, cooling, this traction force was maintained constant while the temperature was gradually reduced below the crystallization point, following a prescribed temperature amplitude. Finally, in the recovery step, the sample was reheated to a temperature above the melting threshold while keeping the external force constant.

Based on the experimental data reported in [47] for the crystalline weight content, the inclusion volume fraction is expressed as a temperature-dependent function, as given by Eqs. (10) and (11). To describe the effects of external loading and thermal conditions on the crystallization process, the effective crystallization and melting temperatures are introduced Eqs. (12) and (13). These effective temperatures play a central role in the model, as they directly determine the evolution of temperature-dependent volume fraction function.

Fig. 7 presents the displacement distribution contour for the 2W shape memory cycle of PCL subjected to an applied stress of 250 kPa. In Fig. 7(a), the material corresponds to shape "A" (as defined in Fig. 2), representing the fully amorphous state at the high temperature (T_h) prior to any applied deformation. Upon applying a constant stress along the x-axis, the sample deforms into shape "B" at high temperature, as shown in Fig. 7(b). The material is then cooled below the crystallization temperature ($T_l < T_C$) under constant stress. During this step, the increase in the crystalline phase enhances both thermal and shape memory strains, resulting in approximately 12% deformation. The temporary shape attained at the end of the cooling, corresponding to point "D" in Fig. 2, is shown in Fig. 7(c). Finally, reheating to the high temperature (T_h) under the same constant stress restores the temporary shape "B", thereby completing the 2W shape memory cycle. Unlike the 1W-SME, this two-way effect allows reversible switching between temporary shapes purely through thermal cycling, without requiring reprogramming.

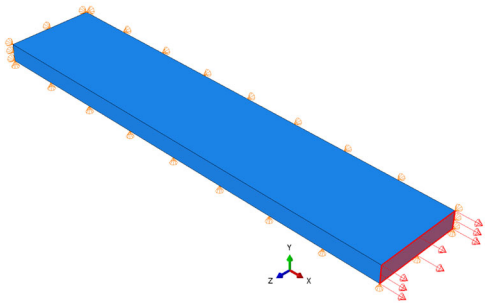

Fig. 6. Geometry and applied boundary condition of the sample in the uniaxial tensile simulation.

Table 1. Material parameters for the PCL in the simulations [34, 48]

E_a (MPa K)	E_c (MPa)	T_C, T_M (℃)	α_a, α_c (1/℃)	ρ_a, ρ_c (kg/m^3)
0.014	900	-15, 20	2, 1.5×10^{-4}	1081, 1195
γ_c^1, γ_m^1 (℃/kPa)	γ_c^2, γ_m^2	β_c, β_m (1/℃^{2})	Υ_c^w	K (W/m℃)
1.65×10^{-4}, -2×10^{-3}	5.5, 8	0.21	23	0.5
C_p (J/kg℃)	β_s (1/MPa)	γ_s	β_s (1/MPa)	T_l, T_h (℃)
1400	1.56×10^5	0.05	1.56×10^5	-40, 65

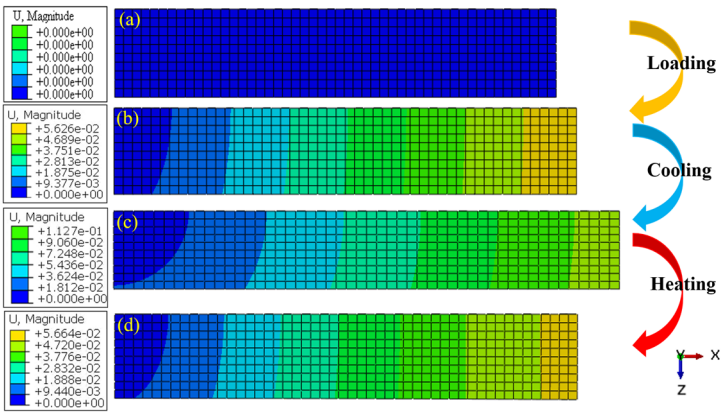

Fig. 7. Displacement distribution contour during shape memory cycle (a) initial shape, (b) deformed shape, (c) temporary shape at the end of cooling, and (d) recovered shape.

Such reversible behavior is crucial for various engineering applications, including smart filters, adaptive windows, artificial muscles, and self-adjusting clamps [9, 10].

As previously described, a shape memory cycle was simulated using ABAQUS to model the quasi-2W-SME under constant external thermomechanical loading. The simulations were conducted at a fixed stress of 250 kPa, with cooling and heating rates set to 2 and 10 °C/min, respectively. The stress-strain-temperature response of PCL under constant stress (250 kPa) is presented in Fig. 8. The strain-temperature curve shows an engineering strain increases approximately 12% as the temperature decreases from 65 to -40 °C. The effect of inclusion size was considered through the aspect ratio a/c = 1/25 in the simulations. The heating–cooling cycle experiences a temperature range of about 105 °C. Notably, during the cooling, the strain increases by about 7% within a 40 °C interval around the crystallization temperature. In contrast, during heating, the crystalline phase remains stable up to its melting point, beyond which the polymer network transforms to an amorphous state, allowing the material to recover its original shape before subsequent cooling. The key differences between the present model and the one-dimensional model by Scalet et al. [34] are related to the influences of shape, size, and interaction of phases. Additionally, improvement in the volume fraction, effective crystallization/melting temperatures, and optimized fitting parameters have enhanced the accuracy of predicting shape memory response. However, the discrepancy (up to 5% at low temperatures) between the predicted and experimental results can be attributed to the inherent complexities of the polymer microstructure. As shown in Fig. 8, the Root Mean Square Error (RMSE) for the predictions obtained from the Scalet et al. [34] model is 2.41, whereas the corresponding value for the proposed model is significantly lower at 0.35. The 85% reduction in RMSE indicates a significant improvement in the prediction accuracy, and its improved agreement with experimental observations.

Fig. 9 compares the predictions of the current model with the experimental data [47] and the Scalet model [34] to assess the effect of ellipsoid inclusion size. To this end, different aspect ratios of the ellipsoidal shape (a/c = 1/5, 1/15, and 1/25) were considered, and the stress-stress-strain-temperature evolution under a fixed external load of 250 kPa during the two-way shape memory cycle is illustrated in Fig. 9. It has been well established that the mechanical and thermal properties of polymeric materials are strongly dependent on their morphological features [49]. Experimental data [44] corresponding to a shape ratio of length/thickness = 23, demonstrated a strong correlation with the model predictions when the inclusion aspect ratio was taken as a/c = 1/25. In this study, for the first time, microstructural characteristics have been considered in investigating the effective properties of 2W-SMP systems. Additionally, the behavior of both phases was assumed to be linear elastic, consistent with existing experimental observations and the existing modeling data.

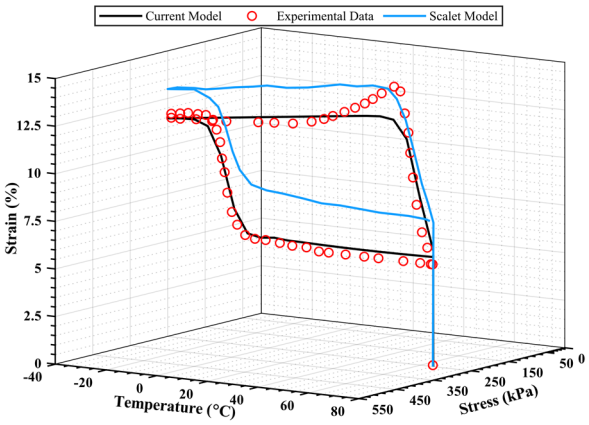

Fig. 8. Evolution of stress-strain-temperature response of PCL: comparison between the present model, experimental data [47], and the Scalet model [34] under a constant stress of 250 kPa.

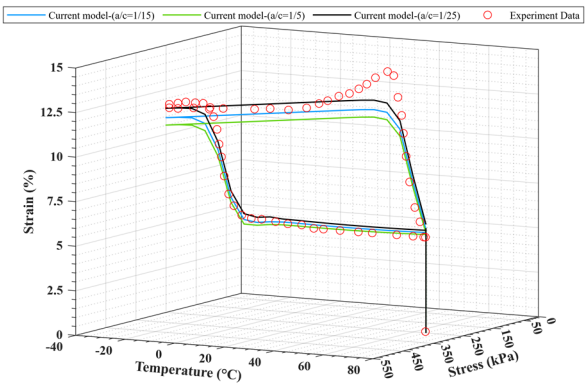

Fig. 9. Influence of ellipsoidal inclusion size effect on shape memory behavior during the programming cycle at 250 kPa, compared with experimental data [47].

The RMSE values for different (a/c) ratios during the cooling phase were 0.64, 0.44, and 0.36, while the corresponding error values during the heating phase were 1.19, 0.87, and 0.62. The reduction in RMSE values across the cooling and heating cycles, from $a/c = 1/5$ to $a/c = 1/25$, indicates an improvement in the results of the proposed model. This improvement reflects a better alignment between the geometric dimensions of the inclusions and their actual morphology, while also highlighting the influence of inclusion phase size in modeling 2W-SMPs. The current model provides a foundation that can be extended in future work to address its limitations. In this study, linear elasticity is assumed for both polymer phases to focus on capturing microstructural effects and interphase interactions, while enabling efficient three-dimensional implementation. Although viscoelastic effects, particularly in the amorphous phase, are relevant, their inclusion would require significantly more complex numerical treatment. Therefore, to preserve clarity and simplicity in this foundational model for 2W-SMPs, such effects are reserved for future model developments.

Fig. 10 presents the strain response of PCL under a constant stress level (250 kPa) for both spherical and ellipsoidal inclusion shapes, compared with the experimental data. As illustrated in Fig. 10, the results obtained from the present model, aligned with experimental findings on the microstructure of semi-crystalline SMPs, demonstrate that ellipsoidal inclusions yield superior predictive accuracy. These findings underscore the critical role of the microstructural and morphological characteristics of the crystalline phase, particularly the size and shape of inclusions, in influencing the shape memory performance of 2W-SMPs. According to Eq. (27), in the initial step when the temperature is constant and the material remains in the amorphous phase, the response follows Hooke's law, and the effective stiffness tensor corresponds to that of the matrix. As cooling begins and the volume fraction of the inclusion phase increases near the crystallization temperature, the crystalline phase increasingly dominates the mechanical response, especially at lower temperatures. Furthermore, during the cooling/heating cycle, the coexistence of two phases with distinct stiffness properties induces disturbance strains, which are effectively captured the proposed model. As depicted in Fig. 10, the RMSE value for ellipsoidal versus spherical inclusions during the cooling step decreases by 52%, from 1.59 to 0.76. Similarly, the corresponding error values during the heating phase are 2.04 for the spherical geometry and 0.64 for the ellipsoidal geometry. These findings underscore the enhanced accuracy of the proposed model when the geometrical representation more closely reflects the actual microstructure. To facilitate analysis, simplified inclusion geometries were employed. Nonetheless, the presented formulation allows for the extraction of the Eshelby tensor corresponding to real microstructure. In this study, idealized inclusion shapes such as ellipsoids were used to capture microstructural effects while maintaining model simplicity and clarity. Although real crystalline morphologies may exhibit more complex geometries, the incorporation of irregular shapes can be pursued in future work due to the additional computational and experimental demands.

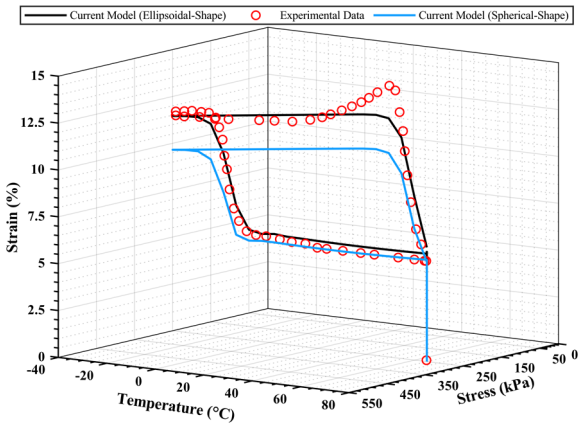

Fig. 10. Comparison of experimental data [47] and simulation results: effect of different inclusion shapes during the shape memory response under 250 kPa.

4. Conclusions

This study developed a micromechanical constitutive model to predict the thermomechanical behavior of quasi-2W shape memory polymers (SMPs) under programming conditions. A 3D micromechanical framework, based on the equivalent inclusion method and a modified Mori-Tanaka approach, was

implemented in ABAQUS via a UMAT subroutine. The key findings are summarized as follows:

- The model incorporates the inclusion phase's shape, size, and volume fraction, along with interaction strains between phases, thereby enabling a more accurate simulation of the shape memory cycle.
- The interaction and disturbance strains were shown to influence the Mori-Tanaka tensor and the effective stiffness—effects typically neglected in prior models.
- Ellipsoidal inclusions more accurately replicate real microstructures compared to spherical ones, with the best agreement for an aspect ratio of approximately 25 (a/c = 1/25).
- Model predictions demonstrated strong agreement with experimental results, validating the importance of microstructural and interaction effects in quasi-2W-SME modeling.
- The proposed model significantly enhances prediction accuracy, achieving up to an 85% reduction in RMSE compared to existing models, and demonstrating superior alignment with experimental data across various loading phases.
- Incorporating ellipsoidal inclusions and refining the a/c ratio led to notable reductions in RMSE during both heating and cooling cycles, confirming the importance of accurate geometric representation in modeling the microstructure of two-way shape memory polymers.

Acknowledgments

Iran National Science Foundation (INSF) is gratefully acknowledged for its financial support of this work (No. 98014929). The authors express their gratitude to the research board of K. N. Toosi University of Technology for their support and provision of research facilities utilized in this study.

Authors' contributions

Meisam Bakhtiari: Formal analysis, Investigation, Software, Data curation, Writing - original draft

Keivan Narooei: Conceptualization, Supervision, Methodology, Software, Writing - review & editing

Conflict of interest

The authors declare that there is no conflict of interest in this research.

Data availability

The data that support the findings of this study are available on request from the corresponding author.

Funding

The authors declare that no funds, grants, or other support were received during the preparation of this manuscript.

5. References

[1] Vaziri, S., & Narooei, K. (2024). Investigation of post-buckling, energy harvesting, and relaxation of shape memory auxetic structure with thermo-visco-hyperelastic modeling. *Iranian Journal of Materials Forming, 11*(3), 28-39. https://doi.org/10.22099/ijmf.2024.51080.1302

[2] Ghorbanoghli, A., & Narooei, K. (2019). A new hyper-viscoelastic model for investigating rate dependent mechanical behavior of dual cross link self-healing hydrogel. *International Journal of Mechanical Sciences*, 159, 278-286. https://doi.org/10.1016/j.ijmecsci.2019.06.019

[3] Fang-Fang, L., & Guo-Liang, L. (2025). Rational molecular Design: Advances in stimuli-responsive shape memory polymers and composites. *European Polymer Journal*, 223, 113642. https://doi.org/10.1016/j.eurpolymj.2024.113642

[4] Hosseinzadeh, M., Ghoreishi, M., & Narooei, K. (2023). 4D printing of shape memory polylactic acid beams: An experimental investigation into FDM additive manufacturing process parameters, mathematical modeling, and optimization. *Journal of Manufacturing Processes*, 85, 774-782. https://doi.org/10.1016/j.jmapro.2022.12.006

[5] He, Q., Zhao, Z., Zhong, Q., Liu, S., Deng, K., Liu, Y., Zhang, N., Zhao, Z., Zhan, F., & Zhao, J. (2024). Switchable shape memory polymer bio-inspired adhesive and its application for unmanned aerial vehicle landing. *Chinese Journal of Aeronautics, 37*(3), 380-390. https://doi.org/10.1016/j.cja.2023.09.032

[6] Hosseinzadeh, M., Ghoreishi, M., & Narooei, K. (2021). An investigation into the effect of thermal variables on the 3D printed shape memory polymer structures with different geometries. *Journal of Intelligent Material Systems and Structures, 33*(5), 715-726. https://doi.org/10.1177/1045389X211028286

[7] Prem Kumar, C., N., S., D., L., Naga, M. R. G., & Vakkalagadda, M. R. K. Shape memory polymers, blends, and composites: processing, properties, and applications. *Polymer-Plastics Technology and Materials,* 1-29. https://doi.org/10.1080/25740881.2025.2460063

[8] Ke, D., Chen, Z., Momo, Z. Y., Jiani, W., Xuan, C., Xiaojie, Y., & Xueliang, X. (2020). Recent advances of two-way shape memory polymers and four-dimensional printing under stress-free conditions. *Smart Materials and Structures, 29*(2), 023001. https://doi.org/10.1088/1361-665X/ab5e6d

[9] Basak, S., & Bandyopadhyay, A. (2022). Two-way semicrystalline shape memory elastomers: development and current research trends. *Advanced Engineering Materials, 24*(10), 2200257. https://doi.org/10.1002/adem.202200257

[10] Scalet, G. (2020). Two-way and multiple-way shape memory polymers for soft robotics: An overview. *Actuators, 9*(1), 10. https://doi.org/10.3390/act9010010

[11] Zeng, H., Sun, H., & Gu, J. (2021). Modeling the one-way and two-way shape memory effects of semi-crystalline polymers. *Smart Materials and Structures, 30*(9), 095020. https://doi.org/10.1088/1361-665X/ac179e

[12] Rashidi, M., & Narooei, K. (2020). Structural mechanics approach to investigate the hyperelastic mechanical behavior of single and multi-wall carbon nanotubes. *Iranian Journal of Materials Forming, 7*(2), 88-103. https://doi.org/10.22099/ijmf.2020.37930.1163

[13] Dolynchuk, O., Kolesov, I., & Radusch, H. J. (2014). Theoretical description of an anomalous elongation during two-way shape-memory effect in crosslinked semicrystalline polymers. *Macromolecular Symposia, 346*(1), 48-58. https://doi.org/10.1002/masy.201400065

[14] Yan, C., Yang, Q., & Li, G. (2020). A phenomenological constitutive model for semicrystalline two-way shape memory polymers. *International Journal of Mechanical Sciences*, 177, 105552. https://doi.org/10.1016/j.ijmecsci.2020.105552

[15] Janbaz, S., Narooei, K., van Manen, T., & Zadpoor, A. A. (2020). Strain rate–dependent mechanical metamaterials. *Science Advances, 6*(25), eaba0616. https://doi.org/10.1126/sciadv.aba0616

[16] Liang, Z., Li, J., Zhang, X., & Kan, Q. (2023). A viscoelastic-viscoplastic constitutive model and its finite element implementation of amorphous polymers. *Polymer Testing*, 117, 107831. https://doi.org/10.1016/j.polymertesting.2022.107831

[17] Liu, Y., Gall, K., Dunn, M. L., Greenberg, A. R., & Diani, J. (2006). Thermomechanics of shape memory polymers: Uniaxial experiments and constitutive modeling. *International Journal of Plasticity, 22*(2), 279-313. https://doi.org/10.1016/j.ijplas.2005.03.004

[18] Srivastava, V., Chester, S. A., & Anand, L. (2010). Thermally actuated shape-memory polymers: Experiments, theory, and numerical simulations. *Journal of the Mechanics and Physics of Solids, 58*(8), 1100-1124. https://doi.org/10.1016/j.jmps.2010.04.004

[19] Bakhtiari, M., & Narooei, K. (2025). A micromechanical model to predict the effective thermomechanical behavior of one-way shape memory polymers. *Mechanics of Materials*, 201, 105230. https://doi.org/10.1016/j.mechmat.2024.105230

[20] Nemat-Nasser, S., & Hori, M., (2013). *Micromechanics: overall properties of heterogeneous materials*. Elsevier.

[21] Voigt, W. (1928). Crystal physics textbook. *Journal of Modern Physics, 9*(4), 80-85.

[22] Reuss, A. (1929). Calculation of the flow limits of mixed crystals on the basis of the plasticity of monocrystals. *Zeitschrift für Angewandte Mathematik und Mechanik, 9*(1), 49-58. https://doi.org/10.1002/zamm.19290090104

[23] Mori, T., & Tanaka, K. (1973). Average stress in matrix and average elastic energy of materials with misfitting inclusions. *Acta Metallurgica, 21*(5), 571-574. https://doi.org/10.1016/0001-6160(73)90064-3

[24] Nemat-Nasser, S., Su, Y., Guo, W. G., & Isaacs, J. (2005). Experimental characterization and micromechanical modeling of superelastic response of a porous NiTi shape-memory alloy. *Journal of the Mechanics and Physics of Solids, 53*(10), 2320-2346. https://doi.org/10.1016/j.jmps.2005.03.009

[25] Kachanov, M., & Sevostianov, I., (2018). *Micromechanics of materials, with applications*. Springer.

[26] Poluektov, M., Freidin, A. B., & Figiel, Ł. (2019). Micromechanical modelling of mechanochemical processes in heterogeneous materials. *Modelling and Simulation in Materials Science and Engineering, 27*(8), 084005. https://doi.org/10.1088/1361-651X/ab3b3a

[27] Baniassadi, M., Baghani, M., & Rémond, Y., (2023). *Applied micromechanics of complex microstructures: Computational modeling and numerical characterization*. Elsevier.

[28] Umer, U., Abidi, M. H., Almutairi, Z., & El-Meligy, M. A. (2024). Micromechanics evaluation of equivalent temperature-dependent stiffness of graphene-reinforced shape memory polymer nanocomposites. *Results in Engineering*, 24, 102978. https://doi.org/10.1016/j.rineng.2024.102978

[29] Tang, T., & Felicelli, S. D. (2015). Micromechanical investigations of polymer matrix composites with shape memory alloy reinforcement. *International Journal of Engineering Science*, 94, 181-194. https://doi.org/10.1016/j.ijengsci.2015.05.008

[30] Guo, Q., & Zaïri, F. (2021). A micromechanics-based model for deformation-induced damage and failure in elastomeric media. *International Journal of Plasticity*, 140, 102976. https://doi.org/10.1016/j.ijplas.2021.102976

[31] Yang, Q., & Li, G. (2016). Temperature and rate dependent thermomechanical modeling of shape memory polymers with physics based phase evolution law. *International Journal of Plasticity*, 80, 168-186. https://doi.org/10.1016/j.ijplas.2015.09.005

[32] Fulati, A., Uto, K., & Ebara, M. (2022). Influences of crystallinity and crosslinking density on the shape recovery force in poly(ε-caprolactone)-based shape-memory polymer blends. *Polymers, 14*(21), 4740. https://doi.org/10.3390/polym14214740

[33] Westbrook, K. K., Mather, P. T., Parakh, V., Dunn, M. L., Ge, Q., Lee, B. M., & Qi, H. J. (2011). Two-way reversible shape memory effects in a free-standing polymer composite. *Smart Materials and Structures, 20*(6), 065010. https://doi.org/10.1088/0964-1726/20/6/065010

[34] Scalet, G., Pandini, S., Messori, M., Toselli, M., & Auricchio, F. (2018). A one-dimensional phenomenological model for the two-way shape-memory effect in semi-crystalline networks. *Polymer,* 158, 130-148. https://doi.org/10.1016/j.polymer.2018.10.027

[35] Gu, J., Wang, C., Zeng, H., Duan, H., Wan, M., & Sun, H. (2024). A thermo-mechanical constitutive model for triple-shape and two-way shape memory polymers. *Smart Materials and Structures, 33*(6), 065034. https://doi.org/10.1088/1361-665X/ad4cc2

[36] Kim, J. H., Kang, T. J., & Yu, W. R. (2010). Thermo-mechanical constitutive modeling of shape memory polyurethanes using a phenomenological approach. *International Journal of Plasticity, 26*(2), 204-218. https://doi.org/10.1016/j.ijplas.2009.06.006

[37] Gilormini, P., & Diani, J. (2012). On modeling shape memory polymers as thermoelastic two-phase composite materials. *Comptes Rendus Mécanique, 340*(4), 338-348. https://doi.org/10.1016/j.crme.2012.02.016

[38] Chen, Y. C., & Lagoudas, D. C. (2008). A constitutive theory for shape memory polymers. Part I: Large deformations. *Journal of the Mechanics and Physics of Solids, 56*(5), 1752-1765. https://doi.org/10.1016/j.jmps.2007.12.005

[39] Smith Jr, K. J. (1983). Crystallization under stress: A theory of fibrillar crystallization. *Journal of Polymer Science: Polymer Physics Edition, 21*(1), 55-63. https://doi.org/10.1002/pol.1983.180210105

[40] Abdul-Hameed, H., Messager, T., Ayoub, G., Zaïri, F., Naït-Abdelaziz, M., Qu, Z., & Zaïri, F. (2014). A two-phase hyperelastic-viscoplastic constitutive model for semi-crystalline polymers: Application to polyethylene materials with a variable range of crystal fractions. *Journal of the Mechanical Behavior of Biomedical Materials*, 37, 323-332. https://doi.org/10.1016/j.jmbbm.2014.04.016

[41] Nguyen, T. L., Bédoui, F., Mazeran, P. E., & Guigon, M. (2015). Mechanical investigation of confined amorphous phase in semicrystalline polymers: Case of PET and PLA. *Polymer Engineering & Science, 55*(2), 397-405. https://doi.org/10.1002/pen.23896

[42] Chen, J. (2021). Advanced electron microscopy of nanophased synthetic polymers and soft complexes for energy and medicine applications. *Nanomaterials*, *11*(9), 2405. https://doi.org/10.3390/nano11092405

[43] Brusselle-Dupend, N., & Cangémi, L. (2008). A two-phase model for the mechanical behaviour of semicrystalline polymers. Part I: Large strains multiaxial validation on HDPE. *Mechanics of Materials, 40*(9), 743-760. https://doi.org/10.1016/j.mechmat.2008.03.011

[44] Bédoui, F., Diani, J., Régnier, G., & Seiler, W. (2006). Micromechanical modeling of isotropic elastic behavior of semicrystalline polymers. *Acta Materialia, 54*(6), 1513-1523. https://doi.org/10.1016/j.actamat.2005.11.028

[45] Mura, T., (2013). *Micromechanics of defects in solids*. Springer Science & Business Media.

[46] Baghani, M., Naghdabadi, R., Arghavani, J., & Sohrabpour, S. (2012). A constitutive model for shape memory polymers with application to torsion of prismatic bars. *Journal of Intelligent Material Systems and Structures, 23*(2), 107-116. https://doi.org/10.1177/1045389X11431745

[47] Pandini, S., Baldi, F., Paderni, K., Messori, M., Toselli, M., Pilati, F., Gianoncelli, A., Brisotto, M., Bontempi, E., & Riccò, T. (2013). One-way and two-way shape memory behaviour of semi-crystalline networks based on sol–gel cross-linked poly(ε-caprolactone). *Polymer, 54*(16), 4253-4265. https://doi.org/10.1016/j.polymer.2013.06.016

[48] Wurm, A., Lellinger, D., Minakov, A. A., Skipa, T., Pötschke, P., Nicula, R., Alig, I., & Schick, C. (2014). Crystallization of poly(ε-caprolactone)/MWCNT composites: A combined SAXS/WAXS, electrical and thermal conductivity study. *Polymer, 55*(9), 2220-2232. https://doi.org/10.1016/j.polymer.2014.02.069

[49] Tencé-Girault, S., Woehling, V., Oikonomou, E. K., Karpati, S., & Norvez, S. (2018). About the art and science of visualizing polymer morphology using transmission electron microscopy. *Macromolecular Chemistry and Physics, 219*(3), 1700483. https://doi.org/10.1002/macp.201700483